

Linking the thermostability of FIP-nha (*Nectria haematococca*) to its structural properties

Yusi Liu^{a,b,c,1}, Shanna Bastiaan-Net^{b,1}, Yuebin Zhang^{d,1}, Tamara Hoppenbrouwers^{b,e}, Yingying Xie^{a,f}, Yulu Wang^a, Xue Wei^a, Guoming Du^a, Haowen Zhang^a, Khandader M.D. Sharif Uddin Imam^a, Harry Wichers^{b,e,*}, Zhen Li^{a,**}

^a Laboratory of Biomufacturing and Food Engineering, Institute of Food Science and Technology, Chinese Academy of Agriculture Sciences, Beijing 100193, China

^b Wageningen Food and Biobased Research, Wageningen University and Research, Wageningen 6708WG, the Netherlands

^c Laboratory of Food Chemistry, Wageningen University, Wageningen 6708WG, the Netherlands

^d State Key Laboratory of Molecular Reaction Dynamics, Dalian Institute of Chemical Physics, Chinese Academy of Sciences, Dalian 116023, China

^e Laboratory of Food Quality and Design, Wageningen University, Wageningen 6708WG, the Netherlands

^f Beijing SeekGene BioSciences Co., Ltd, Beijing 102206, China

ARTICLE INFO

Keywords:

Immunomodulatory proteins
Cytotoxicity
Thermostability
Oligomerization

ABSTRACT

Fungal immunomodulatory proteins (FIPs) have been investigated for their use as potential natural derived anti-tumor molecules. However, the stability of FIPs is critical for their preparation and storage. In this study, the correlation between thermal stability and protein structural features of rFIP-nha, with significant anti-tumor activity, has been evaluated. For comprehensive analysis, FIP-nha and its homologues FIP-gmi, FIP-fve, and LZ-8 were all recombinantly expressed in *E. coli*. In solution, rFIP-nha and rFIP-gmi formed tetramers; rFIP-fve and rLZ-8 appeared as dimers. Their melting temperatures were 85.1 °C, 77.8 °C, 66.5 °C, and 64.4 °C, respectively. Accordingly, their cytotoxicity was also temperature dependent. To investigate the underlying mechanism of their thermostability, we solved the crystal structure of FIP-nha. Detailed structure analysis, molecular dynamic simulation and mutagenesis studies indicated that a higher thermostability was correlated to higher oligomerization states, larger interface area, and more interactions. The structure property studies indicate that Y12, D61 and Y108 were critical for oligomerization and high thermostability of rFIP-nha, but the dimeric and tetrameric states of rFIP-nha exert similar cytotoxicity on A549 cells. Taken together, these findings reveal that thermostability of FIPs was dependent on their oligomerization state, and correlated with their cytotoxicity.

1. Introduction

Fungal immunomodulatory proteins (FIPs), a group of small proteins with notable immunomodulatory activity, have been investigated for their use as a potential anti-tumor drug [1–5]. FIPs were described to directly inhibit tumor growth via inhibition of telomerase activity, induction of apoptosis and autophagy, arrest the cell cycle, as well as inhibition of migration, invasion and metastasis [1,6,7]. LZ-8 (*Ganoderma lucidum*) and FIP-gmi (*G. microsporum*) could exert anti-tumor activity via direct tumor growth inhibition, such as induction of autophagy [8–11] and apoptosis [12–14], cell cycle arrest [15], and inhibition of

migration [16,17] and invasion [18]. Moreover, FIPs could also indirectly inhibit tumor growth via immunomodulatory properties, such as induction of pro or anti-inflammatory cytokine and chemokine secretion, enhancement of cell adhesion molecule expression on T cells and macrophages, and improvement of lymphocyte proliferation [1,19]. FIP-fve (*Flammulina velutipes*) exert its anti-tumor activity via innate and adaptive immunity [20–22]. FIP-nha, cloned from *Nectria haematococca* [23,24], exerts considerable direct anti-tumor activity on human lung cancer A549 cells, human gastric cancer cell lines (AGS, MGC823 and SGC7901 cells), human hepatic cancer HepG2 cells, and human leukemia HL60 cells [25–28]. In-vitro and ex-vivo studies showed that rFIP-

* Corresponding author at: Wageningen Food and Biobased Research, Wageningen University and Research, Wageningen 6708WG, the Netherlands.

** Corresponding author.

E-mail addresses: Harry.Wichers@wur.nl (H. Wichers), lizhen19890911@163.com (Z. Li).

¹ These authors contributed equally to the article.

nha negatively regulated PI3K/Akt signaling, upregulated p53 expression, and induced cell cycle arrest, autophagy, and apoptosis of human lung adenocarcinoma [25,29]. Meanwhile, an in-vitro study suggested that rFIP-nha blocked the EGFR-mediated STAT3/Akt pathway to induce apoptosis and autophagy in human gastric cancer [28].

The thermostability of protein drugs have been proven critical for maintaining their bioactivity during production and storage. Studies showed that thermostability properties relate to several factors, such as oligomerization states, glycosylation states, structural interactions (disulfide bridges, hydrogen bonds, and hydrophobic interaction) and secondary structure (α -helix stability, rigidly or flexibility) [30–32]. For instance, the melting temperature (T_m) of arginine deiminase (an anti-cancer agent for the therapy of arginine-auxotrophic tumors) has been improved from 63.55 °C to 71.01 °C via oligomerization modification [33,34]. The half-life of arginine deiminase was also enhanced from 4 min to 17.5 min at 60 °C via this structural design [33,34]. In addition, the T_m value of anti-PD-L1 antibody drug increased from 47 to 54 °C via glycosylation modification [35]. FIPs are considered as potential anti-tumor drugs, but are not per se stable at high temperatures, which limits their applications. Heating FIP-fve (*Flammulina velutipes*) in water at 60 °C for 5 min reduced its chromatographically detectable amount by 25% [36]. LZ-8 (*Ganoderma lucidum*) was non-reversibly denatured when the temperature was above 55 °C [37]. However, the underlying mechanisms of their thermostability are not clear.

The crystal structures of several FIPs (PDB: LZ-8, 3F3H; FIP-fve, 1OSY; FIP-gmi, 3KCW) have been determined. Their monomeric structures are similar, consisting of an N-terminal α -helix followed by a fibronectin III (FNIII) fold [38–41]. The overall structures of LZ-8 and FIP-fve behave as non-covalently linked homodimers with the interlocking helices in the N-terminus [38,40,41] while FIP-gmi behaved as tetramer, forming a dimer-dimer arrangement [39]. rFIP-nha exerts the most outstanding thermal stability among all the characterized FIPs. However, the mechanisms involved in its thermostability remain unclear. Insights into structural aspects associated with thermostability of FIPs are valuable, as they provide a better understanding of the mechanisms involved in the anti-tumor activity of FIPs, and lay a foundation for enhancement of thermostability of FIPs through structural design. Therefore, in the current study, we tested FIPs oligomeric states via SLS analysis and tested T_m value via DSC analysis. Meanwhile, the cytotoxicity of FIPs and its correlation with their thermostability were evaluated. To gain insight into the thermostability mechanism of rFIP-nha, its crystal structure was determined and compared with FIP-gmi, FIP-fve and LZ-8. The key residues for high thermostability of rFIP-nha were proposed and a mutagenesis study was performed to confirm this hypothesis.

2. Materials and methods

2.1. Materials and chemicals

The plasmid pGEX-6P-1 and *Escherichia coli* BL21 competent cells used for protein expression were purchased from Amersham Pharmacia Biotech (Buckinghamshire, UK) and TransGen Biotech (Beijing, China), respectively. A549 cells were obtained from the Cell Bank of National Biomedical Laboratory, Chinese Academy of Medical Sciences (Beijing, China). The Glutathione Sepharose and Superdex 200 chromatography column were purchased from GE healthcare. Doxorubicin (Adriamycin) HCl was purchased from Selleck. The plasmid of PreScission Protease was kindly provided from Tsinghua University. Other chemicals were purchased from Biolab (Beijing, China).

2.2. Gene and mutagenesis construction of FIPs

The genes encoding FIP-nha (GenBank ID: EEU37941.1), FIP-gmi (GenBank ID: 310942694), FIP-fve (GenBank ID: ADB24832.1) and LZ-8 (GenBank ID: P14945.2) were synthesized by Xianghong

Biotechnology Co., Ltd. (Beijing, China). The mutation Y12T/Q/R, D61N and Y108F variants of FIP-nha were constructed via Quick-change PCR, and the primers (Table S1) were synthesized by Beijing Ruibio BioTech Co., Ltd.

2.3. Protein preparation

Plasmid pGEX-6p-1 carrying the gene of FIP-nha, FIP-gmi, FIP-fve, or LZ-8 between restriction sites BamHI and NotI was transformed into *E. coli* BL21 (DE3). All the recombinant FIPs contained an N-terminal GST tag.

Transformed bacterial colonies were cultured and fermented following the method adapted from Xin L. et al. [42] and Shuying L. et al. [26]. Briefly, transformed bacterial colonies were fermented in 1 L LB media containing 0.2 mM IPTG and 100 μ g/mL ampicillin, shaking in 2 L bottles using an IS-RDS4 incubator shaker (SH Scientific, Portland, American) at 18 °C for 14 h to OD600 of 0.6. The cells were collected by centrifugation at 4 °C (5210 \times g), resuspended in 300 mL PBS (10 mM, pH 7.4), and then lysed using a high-pressure homogenizer (ATS, Weilerswist, Germany). Cell lysates were centrifuged (20,400 \times g) for 50 min at 4 °C and the supernatant was subjected to Glutathione Sepharose columns (GE Healthcare, Uppsala, Sweden) for recombinant protein purification as described by the method of Harper and Speicher for GST fusion protein purification [43]. The GST-tag was removed by PreScission Protease, and the protein was further purified using Superdex-200 (1.6 cm \times 20 cm, GE healthcare) size exclusion chromatography [44]. The molecular weight and purity of rFIPs was analyzed by 15% reducing SDS-PAGE and Image J [45], with protein marker P1017-1 (LABELAD, Beijing, China). After removing endotoxin in accordance with the instructions of the Endotoxin Removal Kit (Yeasen, Shanghai, China), rFIPs (in PBS solution) were quantified by BCA kit (LABELAD, Beijing, China), snap frozen by liquid nitrogen, and then stored at –80 °C.

2.4. Oligomerization state analysis

The oligomerization state of rFIPs in solution was determined via static light scattering (SLS; DynaPro, WYATT technology, England). 100 μ L rFIPs (concentration >1 mg/mL) was injected onto a Superdex 200 chromatography column, with LS signal, UV signal, and DRI signal detection. 10 mM PBS (pH 7.4) was used as elution buffer with a flow-rate of 0.45 mL/min. The molecular weight of each protein was calculated after ASTRA software analysis.

2.5. Thermostability and cytotoxicity measurements

The T_m of rFIPs was determined via a MicroCal PEAQ-DSC instrument. Concentrations of 1.0–2.0 mg/mL of proteins in 10 mM PBS (pH 7.4) were used for the differential scanning calorimetry (DSC) study. The T_m values of rFIPs were measured at a rate of 3 °C/min from 20 °C to 90 °C [46].

To determine cytotoxicity, A549 cells were seeded in a 96-well flat bottom cell culture-treated plate at a density of 1×10^4 per well and cultured in RPMI 1640 (Biological Industries, Beijing, China) supplemented with 10% fetal bovine serum (Biological Industries, Beijing, China), penicillin (100 U/mL), and streptomycin (100 μ g/mL) at 37 °C in a humidified atmosphere with 5% CO₂. After 12 h of culture, the cells were exposed to rFIPs and Doxorubicin, as positive control, with a concentration of 0 μ M, 0.25 μ M, 0.5 μ M, 1 μ M or 2 μ M for 24 h, except for rFIP-fve, for which the concentrations 0 μ M, 1 μ M, 3 μ M, 10 μ M or 30 μ M were used based on a previous study [47]. Subsequently, the cells were exposed to 1 μ M heat-treated rFIPs for 24 h, except for heat-treated rFIP-fve for which 30 μ M was used. In case of rFIP-nha and rFIP-gmi, heat-treatments encompassed 4 °C, 37 °C, 50 °C, 65 °C, 70 °C, 75 °C, 80 °C and 85 °C, with treatments lasting for 5 min, 30 min, 60 min and 120 min. The heat-treatments for rLZ-8 and rFIP-fve were the same except that the highest temperatures (80 and 85 °C) have been omitted.

Cell viability was determined using the CCK-8 cell proliferation and cytotoxicity assay kit (Biolab, Beijing, China) following the manufacturer's instructions. Each experiment was repeated three times, and the viability of the control group was set to 100%.

2.6. Protein crystallization, X-ray data collection, structure determination and refinement

Rough screening for protein crystallization was performed in 24-well plates at 20 °C under 864 reservoir conditions including the PACT, JSCG (QIAGEN), Hampton Research kit, and Wizard classic crystallization series (Rigaku, Washington, USA) using a hanging-drop diffusion method. Each drop contained 1 µL of reservoir buffer and 1 µL of protein (rFIP-nha 5.1 mg/mL). The optimized condition for rFIP-nha crystallization consisted of 4% v/v Tassimate™ pH 5.0 (Hampton Research, USA) and 14% w/v PEG 3350. 50% glycol (v/v) was used to protect the crystal from freezing in liquid nitrogen. The best crystal was transferred to Shanghai Synchrotron Radiation Facility beamline BL17U (Shanghai, China) for high-resolution diffraction data collection. The collected data was processed using the HKL2000 package [48]. Next, the crystal structure of rFIP-nha was deciphered using the structure of LZ-8 from *Ganoderma lucidum* (PDB code: 3F3H) through molecular replacement method by CCP4 [49]. Standard refinement was achieved using PHENIX [50] and Coot [51]. Interfaces of rFIPs were calculated by CCP4 [49]. The hydrogen (H) bonds, salt bridges and assemblies were analyzed by PISA (https://www.ebi.ac.uk/msd-srv/prot_int/pistart.html). Structural graphics images were prepared with PyMOL (<http://www.pymol.org>).

The structure factors and coordinates for the rFIP-nha structure was deposited in the Protein Data Bank (FIP-nha PDB code: 7WDL).

2.7. Molecular dynamic simulations

Molecular dynamic (MD) simulations of homo-tetrameric states of rFIP-nha and rFIP-gmi were performed using Amber package and the amber ff14sb protein force field. The FIP-fve and LZ-8 were also modeled as pseudo-tetrameric states (dimer-dimer state) initially according to our observed rFIP-nha tetrameric assembly. The TIP4PEW water molecules were used to solvate the tetramers with a buffering range of 1.6 nm and NaCl ions were used to neutralize the charges of the simulated systems. All MD simulation systems were initially refined using 500 steepest descent steps before switching to conjugate gradient energy minimization and gradually heated to 350 K within 2 ns simulation time. The positional restraints were exerted on the backbone of the protein with a weight of 10 kcal/mol/Å² during the energy minimization and heating process. Then, the restraints were released gradually within six equilibration steps under constant pressure and temperature (NPT) ensemble. A distance cutoff of 12 Å was used for the Lennard-Jones interactions and the Particle Mesh Ewald (PME) summation method was employed for calculating Coulomb interactions. After the equilibration process, 6 × 3000 ns production runs for rFIP-nha and 6 × 1400 ns production runs for rFIP-gmi were conducted for further analysis. Due to the fast dimer-dimer dissociation events that occurred during our MD simulations for both of FIP-fve and LZ-8 systems at 350 K, the MD simulations were terminated at 500 ns for FIP-fve and 1000 ns for LZ-8. The hydrogen mass repartitioning was set to 4 amu to enable an integration step of 4 fs during the production runs. Structural graphics images were prepared with PyMOL (<http://www.pymol.org>).

3. Results and discussion

3.1. Characteristics of recombinant FIPs

To our knowledge, FIP-nha possesses the most outstanding anti-tumor activity among the currently studied FIPs (Table 2). The mechanisms of FIPs' anti-tumor activity have been studied and summarized in several reviews [1,2,52]. rFIP-nha has been suggested to inhibit tumor

growth by modulating the PI3K/Akt pathway and p53 expression to regulate cell cycle arrest, autophagy, and apoptosis [25,29]. More specifically, rFIP-nha suppressed Akt phosphorylation, leading to G1/S and G2/M cell cycle arrest; rFIP-nha induced p53 up-regulation and PI3K/Akt down-regulation which promoted A549 apoptosis and autophagy [25,29]. To enable the comparison of rFIP-nha with other FIPs (rFIP-gmi, rFIP-fve and rLZ-8), all proteins were expressed recombinantly in *E. coli* and purified. The amino acid sequence identity of FIP-gmi, FIP-fve, and LZ-8 to FIP-nha were 65.1%, 58.6%, and 63.0%, respectively (Fig. 1A). The purity of all the proteins was found to be higher than 95% analyzed on 15% reducing SDS-PAGE (Fig. 1B). To investigate the oligomerization states of rFIPs, gel filtration and SLS analysis was performed [53,54]. As shown in Fig. 1C and Table 1, rFIP-nha and rFIP-gmi formed tetramers, while rFIP-fve and rLZ-8 were dimers in PBS solution.

3.2. Thermal stability of FIPs

To test the thermostability of FIPs, the onset unfolding temperature (T_{Onset}) and the melting temperature (T_m) were measured via DSC. The T_{Onset} of rFIP-nha, rFIP-gmi, rFIP-fve and rLZ-8 were 76.4 °C, 68.7 °C, 57.2 °C, and 53.2 °C, while the T_m were 85.1 °C, 77.8 °C, 66.5 °C, and 64.4 °C, respectively (Fig. 2B).

To analyze the correlation between thermostability and bioactivity of proteins after heat treatment, the cytotoxicity of rFIPs on human lung adenocarcinoma A549 cells were determined. rFIP-nha, rFIP-gmi, rFIP-fve and rLZ-8 displayed a dose-dependent cell viability inhibition on A549 cells, which corroborated previous studies [15,25,26,47,55] (Fig. 2B; Table 2). rFIP-nha displayed the lowest IC50 on A549 cells of all reported FIPs (Table 2) and its cytotoxicity was even higher than that of the anti-tumor drug doxorubicin [56–58]. After heat treatment, the cytotoxicity of rFIPs on A549 cells remained stable when the temperature was much lower than the T_{Onset} ; the cytotoxic activity of the rFIPs decreased or disappeared when the temperature came near the T_{Onset} or exceeded the T_m value (Fig. 2C, D, E, F). Upon heating above the T_{Onset} , protein denaturation occurred. The bioactivity of FIPs was diminished during heat treatment, which was in line with the thermostability assay. Of note, rFIP-nha maintained its biological activity on A549 cells after heating at 80 °C for 1 h. We proposed that rFIP-nha assumes a dimeric state when the temperature was higher than the T_{Onset} and dimeric rFIP-nha might exert cytotoxicity during 80 °C. Then the protein's bioactivity was lost, which might result from protein unfolding or dissociation of the dimer towards a monomeric state.

From this experiment we concluded that heat treatment, and thus likely protein unfolding, had a direct influence on FIPs' cytotoxicity on A549 cells. Thermostability has been investigated for several types of FIPs. A previous study on native FIP-fve extracted from the *Flammulina* mushroom itself showed that heating FIP-fve in water at 60 °C for 5 min resulted in a 25% reduction of FIP-fve [36], which corresponds to our findings. rLZ-8 was found to be irreversibly denatured by temperatures above 55 °C [37], which is also in line with our conclusion. However, one previous study mentioned that FIP-gmi was less thermostable than LZ-8, but no method nor measurement data were shown to substantiate this [39]. We measured that the T_{Onset} and T_m values of rFIP-gmi were 67.1 °C and 77.7 °C respectively, indicating that rFIP-gmi was more thermostable than LZ-8 but less thermostable than rFIP-nha in our study. Combining these results indicates that rFIP-nha exerts the highest thermostability among reported FIPs.

3.3. Thermostability-governing mechanism

3.3.1. Overall protein structure

To better understand the mechanism governing thermostability, we analyzed the overall structure of FIP-gmi (PDB: 3KCW), FIP-fve (PDB: 1OSY), and LZ-8 (PDB: 3F3H). Since the crystal structure of FIP-nha had not yet been determined, its crystallographic assembly and analysis was performed. (Table S3). We obtained high-quality X-ray diffraction data

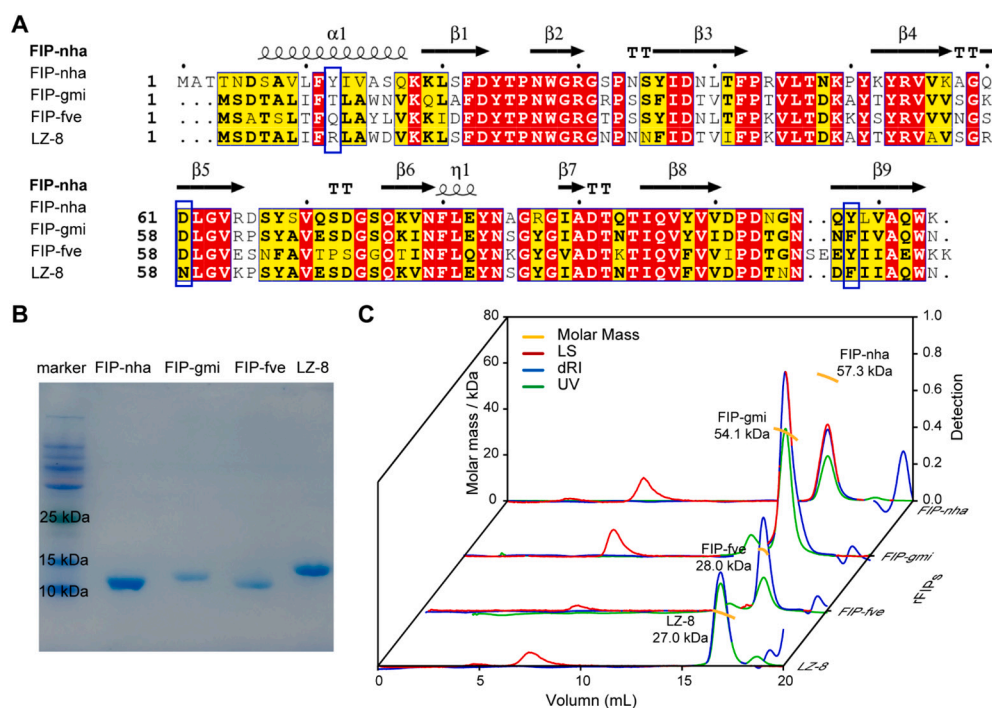


Fig. 1. Characteristics of rFIPs. A. Sequence alignment of FIPs via ESPript (<http://espript.ibcp.fr/ESPript/cgi-bin/ESPript.cgi>). The secondary structure of FIP-nha was analyzed via ESPript; α , β , η , TT represent respectively the α -helix, β sheets, the three amino acid α -helix and β -turns; Y12, D61, Y108 of FIP-nha, labeled with blue squares, were believed to contribute to tetrameric structure and thermostability (see Section 3.3.3 and Fig. 3); B. 15% reducing SDS-PAGE of rFIPs, with 2–5 μ M rFIPs loaded in each well; C. SLS of rFIPs, the molar mass of rFIPs were determined with help of UV (green lines), LS (red lines) and dRI (blue lines) detection going through Superdex 200 chromatography. The vertical axis to the right indicates the UV detection. (For interpretation of the references to colour in this figure legend, the reader is referred to the web version of this article.)

Table 1

Oligomerization characteristics of rFIPs as determined by gel filtration, SLS and PISA analysis.

FIPs	Gel filtration	SLS	PISA
rFIP-nha	Tetramer	Tetramer	Tetramer
rFIP-gmi	Tetramer	Tetramer	Tetramer
rFIP-fve	Dimer	Dimer	Dimer
rLZ-8	Dimer	Dimer	Dimer

for rFIP-nha crystals, with 1.9 Å resolution (Fig. S1), and the structure assembly was elucidated by molecular replacement using LZ-8 as template. The final R-free/R-work was 20.69%/17.50%, which meets the quality requirement of PDB Validation [59]. The overall structure of rFIP-nha consisted of two homodimers in a face-to-face conformation stabilized by non-covalent and hydrophobic interactions (Fig. 3A, I, J). Each molecule of FIP-nha consisted of an N-terminal α -helix followed by a fibronectin III (FNIII) fold. The N-terminal α -helix is important for non-covalent oligomer formation; loop regions of the FNIII fold, of which those in FIP-nha are more similar to those in LZ-8 than in FIP-fve, might be responsible for the anti-tumor activity [38]. Key residues of the FNIII fold could contribute to carbohydrate binding motifs, which might be significant for cytokine induction in immune cells [19,60]. Regarding rFIP-gmi, there is one molecule in its asymmetric unit [39], while rFIP-gmi adopted a tetramer state in buffer (Fig. 1C). Therefore, the biological assembly of rFIP-gmi should be tetramer. To clarify, protein assembly in the asymmetric unit does not represent the oligomer in solution. Differences in the oligomerization state between the crystal asymmetric unit and biological assembly might be expected and does occur in some structures [39,61,62].

3.3.2. Interaction analysis

To explain mechanisms behind the thermostability of the studied rFIPs, we performed a detailed analysis of the structural interface, assemblies and interaction forces of their oligomeric states (Table 3, Fig. 3). As shown in Fig. 3A and B, the interface of rFIP-nha and rFIP-gmi consisted of interface a (an interface in the dimer) and interface b (an interface in between the two dimers). This differed from the interfaces of

FIP-fve and LZ-8, which only consisted of interface a (an interface in the dimer). The interface of rFIP-nha, consisting of interface a and interface b, was the largest, with about 6099.1 Å²; followed by rFIP-gmi, for which the interface area was 5919.9 Å². As expected, the interfaces of FIP-fve and LZ-8 (interface a only) were smaller with 3362.1 Å² and 3285.1 Å², respectively. Meanwhile, the solvation free energy gain upon formation of the assembly (ΔG^{int}) and the free energy of assembly dissociation (ΔG^{diss}) were listed in Table 3.

Subsequently, the detailed interaction forces between these interfaces in different rFIPs were analyzed, including H bonds, salt bridges and hydrophobic interactions. The interaction bonds in rFIP-nha consisted of 41 H bonds and 5 salt bridges, as a total number in the interfaces a and b (Fig. 3I, J and Table S4, S5). There were 36 total H bonds in rFIP-gmi, with no salt bridges (Table S6). With regard to the dimeric FIPs, there were only 7 H bonds, or 9 H bonds in the interface of FIP-fve (Table S7) or LZ-8 (Table S8), respectively. Obviously, FIP-fve and LZ-8 had less inter-subunit interactions compared to rFIP-nha and rFIP-gmi. In general, a higher number of molecular interactions corresponds to a higher binding energy [63,64], substantiating the thermostability of rFIP-nha. As shown in Fig. 3E and F, the interface of rFIP-nha was more hydrophobic than the interface of rFIP-gmi, which also contributes to the thermostability of rFIP-nha. Meanwhile, the hydrophobic interaction within the FIP-fve crystal structure (Fig. 3G) should be much stronger than for LZ-8 (Fig. 3H), which could outweigh the fewer H bonds and result in a higher T_m value. Thus, these findings are in line with the thermodynamic stability data, indicating that rFIP-nha indeed should, structurally, be more stable than other FIPs.

3.3.3. MD simulation of rFIP-nha tetrameric state and site-directed mutagenesis study

In order to further elucidate the molecular mechanism maintaining the structural and thermal stability of the tetrameric assembly of rFIP-nha, MD simulations were performed for both tetrameric states of rFIP-nha and rFIP-gmi at 350 K. The pseudo-tetrameric states (dimer-dimer assembly) of FIP-fve and LZ-8 were also constructed initially, according to our observed FIP-nha tetrameric assembly, for comparison. As shown in Fig. 4, the tetrameric assembly of rFIP-nha exhibits extreme structural stability during our total series of 6 × 3000 ns MD simulations

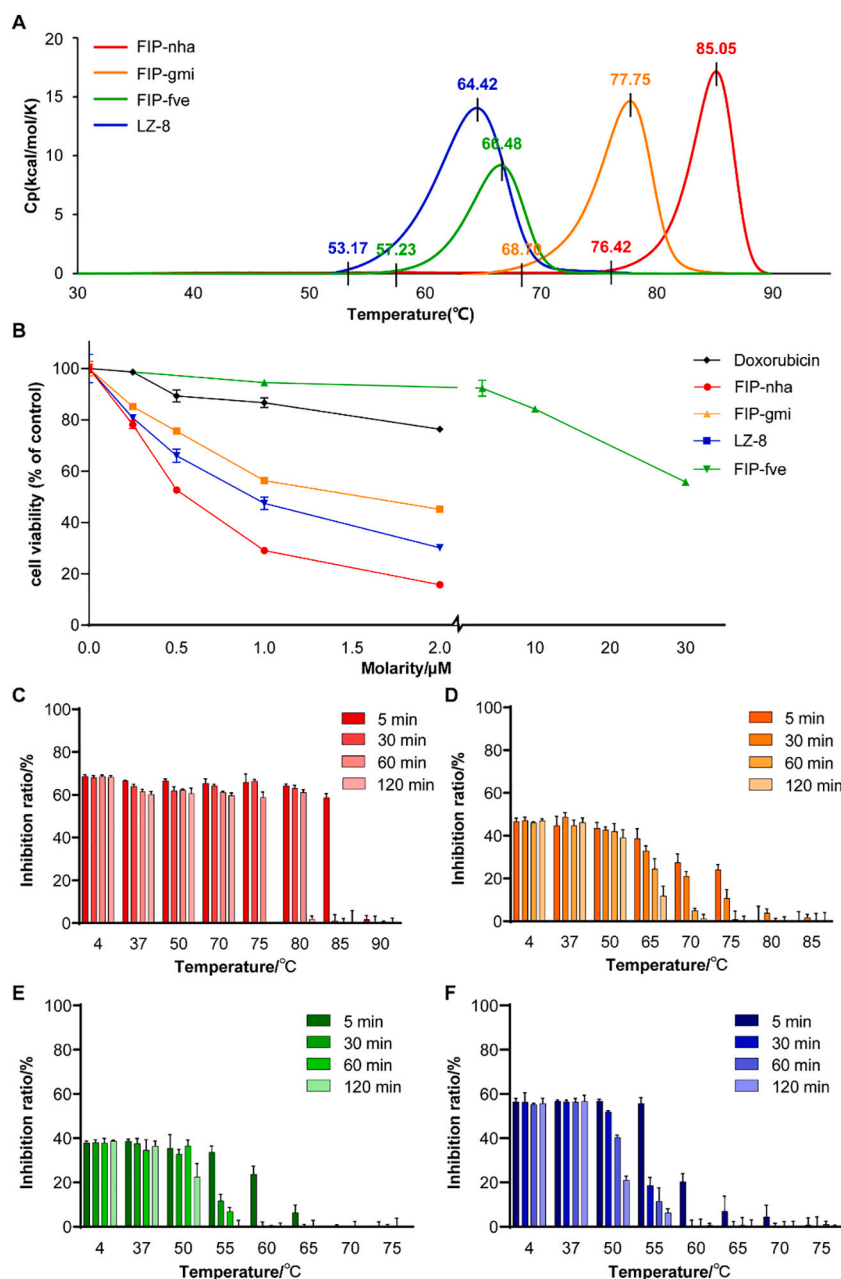


Fig. 2. Biological activity and thermal stability of rFIPs. A. T_m value and T_{onset} of rFIPs, heat capacity value was measured via DSC with temperature increase; B. Cell viability of A549 cells after rFIPs and Doxorubicin treatment; C–F. Impact of thermal treatments on rFIP's cytotoxicity on A549 cells in vitro; the concentration of rFIPs: C. 1 μ M rFIP-nha; D. 1 μ M rFIP-gmi; E. 1 μ M rLZ-8; F. 30 μ M rFIP-fve.

at 350 K. Six individual replicas demonstrated similar narrow root-mean-square deviation (RMSD) distributions of the C-alpha atoms of the tetramer with peaks less than 2.5 Å. In contrast, four of our six MD simulations showed broad RMSD distributions within 1400 ns MD simulation time in rFIP-gmi and only two of the MD simulation trajectories maintained the conformations of the initial tetrameric assembly with RMSD distribution centers around 2.8 Å. These simulations are consistent with our DSC results that rFIP-nha is more thermostable than rFIP-gmi. On the contrary, both FIP-fve and LZ-8 were not able to sustain the tetrameric assembly during our MD simulations at 350 K. The pseudo-tetrameric initial states dissociated into two stable dimeric forms within 500 ns for FIP-fve and 1000 ns for LZ-8 in our MD simulations, which were also in line with the homo-dimeric forms observed in their biological assembly in crystals, rather than the tetrameric assembly. To further identify the key residues responsible for maintaining the

tetrameric assembly of rFIP-nha, molecular mechanics/generalized Born surface area (MM/GBSA) binding free energy decomposition per residue analyses were performed and compared with that of LZ-8 in its dimeric form. We found that, in the case of FIP-nha, N5, S7, F10, Y11, F43, K49, Y108, and L109 played key roles in maintaining the dimerization. These interfaces were also conserved in LZ-8. In addition, the Y12, D61 and Y108 were crucial for the tetrameric assembly in FIP-nha whereas the interactions were absent in the case of the dimeric state of LZ-8, indicating these three sites would be essential to sustain the tetrameric assembly in FIP-nha.

To confirm the importance of the Y12, D61 and Y108 residues within the rFIP-nha structure, we constructed three kinds of genetic variants. Based on the sequence alignment displayed in Fig. 1C, three mutants were created in which the counterpart amino acids in FIP-nha were replaced by those of FIP-gmi, FIP-fve and LZ-8 (Y12T/Q/R + D61N +

Table 2

FIPs that have shown cytotoxicity on A549 cells.

FIPs	IC50 on A549 cells (μM)	Anti-tumor mechanism	Reference
FIP-nha	0.5 ^b	Cell cycle arrest (G1/S and G2/M); apoptosis; autophagy	[25]
FIP-lrh	0.6	–	[68]
FIP-gts	>0.6 ^a	Anti-telomerase effects; ER stress-induced intracellular calcium level; cellular senescence; cell cycle arrest (G1)	[69,70]
FIP-sch2	0.8	Apoptosis; inhibited migration	[71]
LZ-8	1.1 ^b	Cell cycle arrest (G1)	[15]
FIP-dsp2	1.2	Apoptosis; inhibition of migration	[72]
FIP-gmi	1.9 ^b	Cell cycle arrest (G2/M); autophagy	[12,55]
FIP-gap1	2.4 ^a	–	[73]
FIP-bbo	2.6 ^a	Apoptosis; inhibition of migration	[74]
FIP-gsi	4.0 ^a	–	[75]
FIP-gap2	4.9 ^a	–	[73]
FIP-fve	>30.0 ^b	Cell cycle arrest (G1/S); not apoptosis; inhibited migration; suppress proliferation	[47]

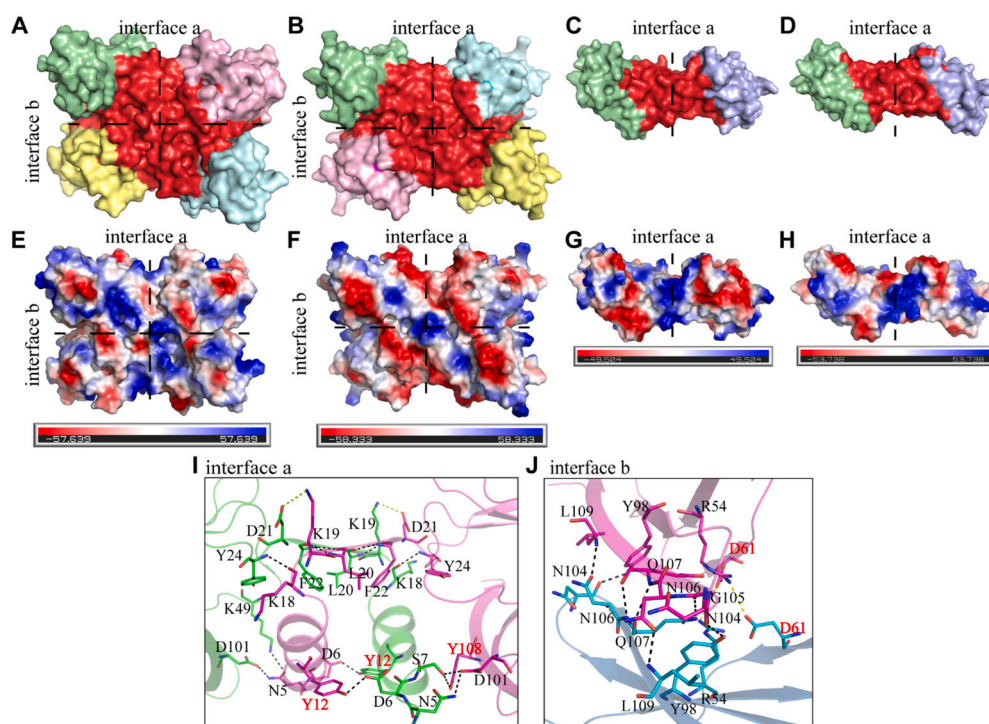
^a Indicates that the IC50 was calculated by concentration (mg/mL) and molecular weight (kDa).^b Indicates that the IC50 was obtained in this study.

Fig. 3. Structural analysis of rFIPs. A, B, C, D structure of rFIP-nha, rFIP-gmi, rFIP-fve, and rLZ-8 shown in surface representation were generated by Pymol, colored by chain respectively, with interface shown in red; E, F, G, H electrostatic surface presentations of rFIP-nha, rFIP-gmi, rFIP-fve, and rLZ-8 were generated by PyMOL, with red (electronegativity) and blue (electro-positivity) representing hydrophilic, and white representing hydrophobic interactions; I, J interaction bonds in rFIP-nha's interface a and interface b; related amino acid residues are labeled with letter and position (Y12, D61, Y108 in red, others in black), and H bonds are shown in dotted black lines, salt bridges are shown in dotted yellow lines. (For interpretation of the references to colour in this figure legend, the reader is referred to the web version of this article.)

Table 3

Overall analysis of FIPs' interface, interactions and assemblies.

FIPs	Total area(\AA^2)	Interface(\AA^2)	Total area/ Interface	ΔG^{int} (kcal/mol)	ΔG^{diss} (kcal/mol)	H bonds	Salt bridges
rFIP-nha	20,897.6	6099.1	3.43	–51.9	6.8	41	5
rFIP-gmi	20,182.8	5919.9	3.41	–60.6	0.9	36	0
FIP-fve	11,471.0	3362.1	3.41	–27.6	19.1	7	0
rLZ-8	11,232.2	3285.1	3.42	–29.2	21.6	9	0

 ΔG^{int} indicates the solvation free energy gain upon formation of the assembly. ΔG^{diss} indicates the free energy of assembly dissociation.

Y108F): FIP-nha 3M-T (based on FIP-gmi), 3M-Q (based on FIP-fve), and 3M-R (based on LZ-8) (Fig. 5A). An SLS analysis suggested that rFIP-nha 3M-T was in a tetrameric state, while rFIP-nha 3M-R and rFIP-nha 3M-Q possessed dimeric states (Fig. 5B). These results suggest that Y12 is the key factor for tetramerization of rFIP-nha. The T_m value of rFIP-nha 3M-T was higher than that of rFIP-nha 3M-Q, and higher than that of rFIP-nha 3M-R (Fig. 5C), which correlated with the T_m value of rFIP-gmi,

rFIP-fve, and rLZ-8. Of note, the oligomerization state of rFIP-nha still related to its thermostability. The thermostability of rFIP-nha and its 3M-T variant (tetrameric) were higher than the thermostability of the dimeric 3M-Q and 3M-R mutants. However, the rFIP-nha 3Ms had an overall lower thermostability than the investigated native FIPs. These observations suggest that Y12, D61 and Y108 are all important for the thermostability of rFIP-nha, and that the three mutations might cause

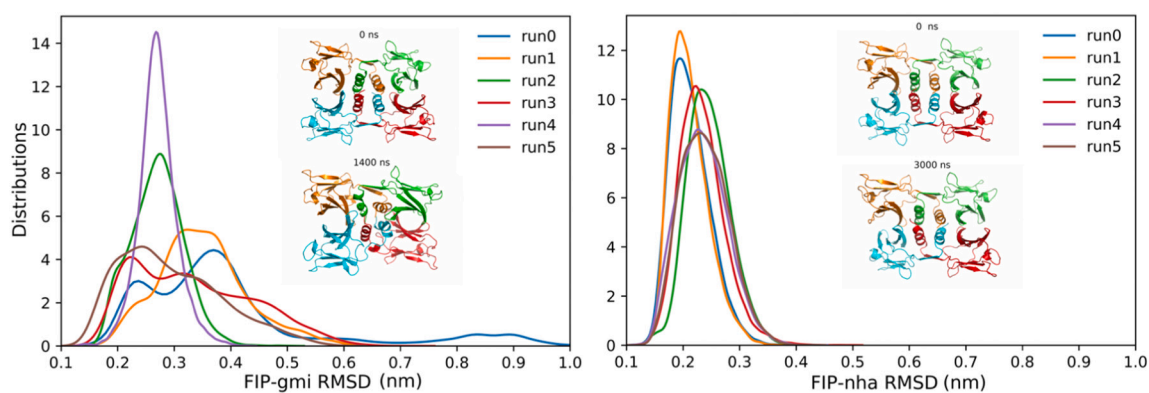


Fig. 4. C-alpha RMSD distributions for tetrameric states of both rFIP-gmi and rFIP-nha from our MD simulations. Six individual runs were performed and the representative snapshots before and after production simulations were shown in the inserted panels. In the case of rFIP-gmi (left panel), four of our six MD simulations showed broad RMSD distributions within 1400 ns and only two of the MD simulation trajectories maintained the conformations with RMSD distribution centers around 2.8 Å. However, all of the MD simulations of the tetrameric assembly of rFIP-nha demonstrated narrow RMSD distributions with peaks less than 2.5 Å (right panel), indicating the structural stability of rFIP-nha in tetrameric state.

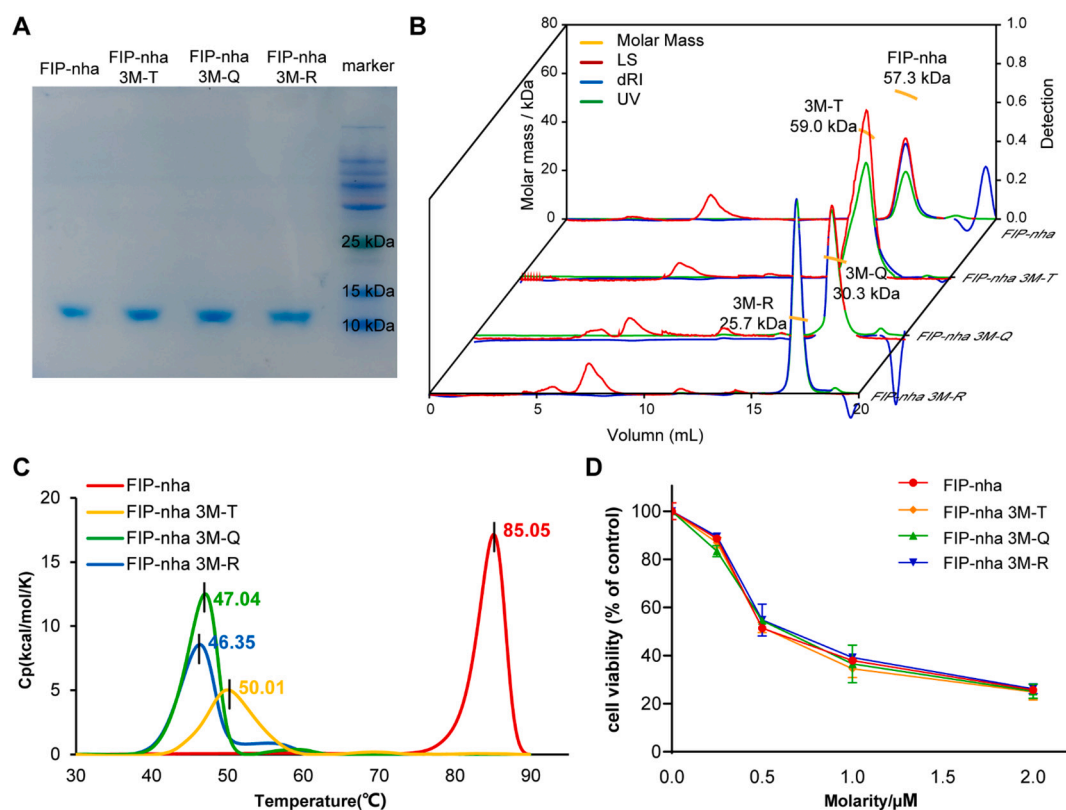


Fig. 5. Amino acid replacement mutants of rFIP-nha. A. 15% reducing SDS-PAGE of rFIP-nha variants with 4–5 µM loaded; B. SLS of rFIP-nha 3Ms, molar mass of rFIPs were determined with help of UV (green lines), LS (red lines) and dRI (blue lines) detection; C. T_m value of rFIP-nha 3Ms, heat capacity value was measured via DSC with temperature increase; D. cell cytotoxicity test of rFIP-nha 3Ms on A549 cells. (For interpretation of the references to colour in this figure legend, the reader is referred to the web version of this article.)

structural changes that destabilize rFIP-nha. The cell viability test of rFIP-nha 3Ms on A549 cells suggested that dimerized rFIP-nha exerts the same cytotoxicity as the tetramer (Fig. 5D). Thus, we speculate that the dimerized rFIP-nha maintains its cytotoxicity at 80 °C for at least an hour (Fig. 3C). During heat treatment, tetrameric rFIP-nha might separate into dimers firstly. Next to the tetrameric state, also the dimeric state of rFIP-nha might be significant for tumor cytotoxicity. Previous studies suggested that the dimerization state of FIPs may play a vital role in their activity [65,66]. The monomer of rFIP-gts did not induce cytokine production on human peripheral blood lymphocytes [65,66]. Also,

the immunomodulatory activity of LZ-8 was impacted by three key residues (L10, W12, and D45) in the interface, that maintains its dimerization via electrostatic interaction [67].

4. Conclusions

In this study, we characterized the anti-tumor protein FIP-nha (*Nectria haematococca*) with high thermostability via detailed structure analysis, molecular dynamics simulation, and mutagenesis studies. Compared with rFIP-gmi, rFIP-fve, and rLZ-8, the thermostability of

rFIP-nha was high, with T_m of 85.1 °C, which might relate to its oligomerization state. To analyze the relation between oligomerization and thermostability of FIPs, we determined the crystal structure of rFIP-nha by molecular replacement method and refined it to 1.9 Å resolution. The overall structure of rFIP-nha consisted of two homodimers in a face-to-face conformation via non-covalent interaction. The tetrameric rFIP-nha and rFIP-gmi have larger intra-molecular interface, stronger interaction force and higher thermostability than the dimeric rLZ-8 and rFIP-fve. MD simulations suggested that rFIP-nha was the most thermostable among the investigated FIPs, and that the amino acids Y12, D61 and Y108 located in the interface, seem to be vital for tetramer formation and thermostability of rFIP-nha. Characterization of replacement mutants (rFIP-nha 3M-T, 3M-Q, and 3M-R) further confirmed the importance of these residues and the relation between oligomerization and thermostability in rFIP-nha. Meanwhile, the cytotoxicity of the mutants showed no obvious difference compared with rFIP-nha, indicating that at least a dimeric structure is pivotal for executing bioactivity and that a tetrameric state does not reduce or increase its cytotoxicity for tumor cells. Our results reveal the mechanisms involved in thermostability of rFIP-nha and provide valuable insights into the regulation mechanism and future application of FIPs.

Ethics statement

This article does not contain any studies with human participants or animals performed by any of the authors.

CRedit authorship contribution statement

Yusi Liu: Writing - original draft & editing, Conceptualization, Methodology, Software, Investigation, Resources. **Shanna Bastiaan-Net:** Writing - original draft & editing, Validation, Methodology, Investigation, Resources. **Yuebin Zhang:** Writing - original draft, Conceptualization, Methodology, Investigation. **Tamara Hoppenbrouwers:** Writing - review & editing, Validation, Methodology, Investigation. **Yingying Xie:** Writing - review & editing, Validation, Methodology, Investigation. **Yulu Wang:** Conceptualization, Methodology, Software, Investigation. **Xue Wei:** Conceptualization, Methodology, Software. **Haowen Zhang:** Methodology, Software. **Guoming Du:** Methodology, Software. **Khandaker MD Sharif Uddin Imam:** Methodology, Resources. **Harry Wichers:** Supervision, Project administration, Writing - review & editing. **Zhen Li:** Supervision, Project administration, Writing - review & editing.

Declaration of competing interest

The authors declare that they have no conflict of interest.

Data availability

Data will be made available on request.

Acknowledgement

This work was supported by the foundation of the National Key Research and Development Plan ‘modern food processing and food storage and transportation technology and equipment’ (Grant number 2017YFD0400204), and the Dutch Ministry of Agriculture Nature and Food Quality via the knowledge- and innovation KB37 program ‘Healthy and Safe food systems’ (Grant number KB-37-001-007). We thank the Shanghai Synchrotron Radiation Facility (SSRF) and the Tsinghua University Branch of China National Center for Protein Sciences (Beijing, China) for providing the facility support of crystallographic data collection, protein characterization and process. We thank prof. dr. Fengjiao Xin for the nice suggestions on the manuscript. We also thank colleagues in/from the lab, Xueyan Yao, Shujun Liu, Miao Chen and

Haiyan Yu, for their cooperation on crystal screen and optimization.

Appendix A. Supplementary data

Supplementary data to this article can be found online at <https://doi.org/10.1016/j.ijbiomac.2022.05.136>.

References

- [1] Q. Li, Y. Zheng, X. Zhou, Fungal immunomodulatory proteins: characteristic, potential antitumor activities and their molecular mechanisms, *Drug Discov. Today* 24 (1) (2018) 307–314.
- [2] P.T. Uribe-Echeverry, G.A. Lopez-Gartner, Fungal immunomodulatory proteins in the context of biomedicine, *Front. Biosci.* 9 (2) (2017) 286–306.
- [3] Q. Li, X. Wang, X. Zhou, Recent status and prospects of the fungal immunomodulatory protein family, *Crit. Rev. Biotechnol.* 31 (4) (2011) 365–375.
- [4] W.C. Xuanwei Zhou, Method for Preparing Intragenus Recombinant Fungal Immunomodulatory Proteins And Application of Intragenus Recombinant Fungal Immunomodulatory Proteins, Qianling Mountains Health Pharmaceutical Industry Technology Co., Ltd., 2015.
- [5] X.W. Xuanwei Zhou, Qizhang Li, Kaiqi Su, Weiran Cong, Gene of Recombinant Fungal Immunomodulatory Protein Between Ganodermas, Protein Coded Thereby, And Application Thereof, Shanghai Jiaotong University, 2013.
- [6] T.-T.W. Tzu-Chih Chen, in: E.P. Office (Ed.), *Fungal Immunomodulatory Protein for Use in the Treatment of Cancer*, Yeastern Biotech Co Ltd, 2016.
- [7] F.X. Shuying Li, Fengzhong Wang, Zhonghao Jiang, Lichao Sun, Ying Huang, Xin Liu, Fungal Immunomodulatory Protein FIP-sch3 With Antitumor Activity, Institute of Food Science and Technology of CAAS, China, 2019.
- [8] I.L. Hsin, C.C. Ou, T.C. Wu, M.S. Jan, M.F. Wu, L.Y. Chiu, K.H. Lue, J.L. Ko, GMI, an immunomodulatory protein from *Ganoderma microsporum*, induces autophagy in non-small cell lung cancer cells, *Autophagy* 7 (8) (2011) 873–882.
- [9] I.L. Hsin, G.T. Sheu, M.S. Jan, H.L. Sun, T.C. Wu, L.Y. Chiu, K.H. Lue, J.L. Ko, Inhibition of lysosome degradation on autophagosome formation and responses to GMI, an immunomodulatory protein from *Ganoderma microsporum*, *Br. J. Pharmacol.* 167 (6) (2012) 1287–1300.
- [10] L.Y. Chiu, M.E. Hu, T.Y. Yang, I.L. Hsin, J.L. Ko, K.J. Tsai, G.T. Sheu, Immunomodulatory protein from *Ganoderma microsporum* induces pro-death autophagy through akt-mTOR-p70S6K pathway inhibition in multidrug resistant lung cancer cells, *PLoS One* 10 (5) (2015), e0125774.
- [11] C. Liang, H. Li, H. Zhou, S. Zhang, Z. Liu, Q. Zhou, F. Sun, Recombinant Lz-8 from *Ganoderma lucidum* induces endoplasmic reticulum stress-mediated autophagic cell death in SGC-7901 human gastric cancer cells, *Oncol. Rep.* 27 (4) (2012) 1079–1089.
- [12] I.-L. Hsin, C.-C. Ou, M.-F. Wu, M.-S. Jan, Y.-M. Hsiao, C.-H. Lin, J.-L. Ko, GMI, an immunomodulatory protein from *Ganoderma microsporum*, potentiates cisplatin-induced apoptosis via autophagy in lung cancer cells, *Mol. Pharm.* 12 (5) (2015) 1534–1543.
- [13] S.Y. Huang, C.C. Chien, R.S. Hseu, V.Y.J. Huang, S.Y. Chiang, C.J. Huang, S. K. Chen, R.Y. Tsai, H.T. Lin, Y.C. Cheng, *Ganoderma microsporum* immunomodulatory protein induces apoptosis and potentiates mitomycin C-induced apoptosis in urinary bladder urothelial carcinoma cells, *J. Cell. Biochem.* 119 (6) (2018) 4592–4606.
- [14] T.Y. Lin, W.J. Hua, H. Yeh, A.J. Tseng, Functional proteomic analysis reveals that fungal immunomodulatory protein reduced expressions of heat shock proteins correlates to apoptosis in lung cancer cells, *Phytomedicine* 80 (2021), 153384.
- [15] C.-T. Wu, T.-Y. Lin, H.-Y. Hsu, F. Sheu, C.-M. Ho, E.I.-T. Chen, Ling Zhi-8 mediates p53-dependent growth arrest of lung cancer cells proliferation via the ribosomal protein S7-MDM2-p53 pathway, *Carcinogenesis* 32 (12) (2011) 1890–1896.
- [16] C.T. Lu, P.Y. Leong, T.Y. Hou, S.J. Huang, Y.P. Hsiao, J.L. Ko, *Ganoderma* immunomodulatory protein and chidamide down-regulate integrin-related signaling pathway result in migration inhibition and apoptosis induction, *Phytomedicine* 51 (2018) 39–47.
- [17] R.-I. You, W.-S. Wu, C.-C. Cheng, J.-R. Wu, S.-M. Pan, C.-W. Chen, C.-T. Hu, Involvement of N-glycan in multiple receptor tyrosine kinases targeted by Ling-Zhi-8 for suppressing HCC413 tumor progression, *Cancers (Basel)* 11 (1) (2018).
- [18] C.-H. Lin, G.-T. Sheu, Y.-W. Lin, C.-S. Yeh, Y.-H. Huang, Y.-C. Lai, J.-G. Chang, J.-L. Ko, A new immunomodulatory protein from *Ganoderma microsporum* inhibits epidermal growth factor mediated migration and invasion in A549 lung cancer cells, *Process Biochem.* 45 (1537–1542) (2010).
- [19] Y. Liu, S. Bastiaan-Net, H. Wichers, Current understanding of the structure and function of fungal immunomodulatory proteins, *Front. Nutr.* 7 (2020) 132.
- [20] H.-H. Chang, K.-Y. Hsieh, C.-H. Yeh, Y.-P. Tu, F. Sheu, Oral administration of an *Enoki* mushroom protein FVE activates innate and adaptive immunity and induces anti-tumor activity against murine hepatocellular carcinoma, *Int. Immunopharmacol.* 10 (2) (2010) 239–246.
- [21] P.H. Wang, C.I. Hsu, S.C. Tang, Y.L. Huang, J.Y. Lin, J.L. Ko, Fungal immunomodulatory protein from *Flammulina velutipes* induces interferon-gamma production through p38 mitogen-activated protein kinase signaling pathway, *J. Agric. Food Chem.* 52 (9) (2004) 2721–2725.
- [22] Y. Ding, S.V. Seow, C.H. Huang, L.M. Liew, Y.C. Lim, I.C. Kuo, K.Y. Chua, Coadministration of the fungal immunomodulatory protein FIP-Fve and a tumour-associated antigen enhanced antitumour immunity, *Immunology* 128 (1 Suppl) (2009) e881–e894.

- [23] H.Z. Bin Yao, Shuying Li, Huiying Luo, Kun Meng, Peilong Yang, Yaru Wang, Huoqing Huang, Pengjun Shi, Tiezheng Yuan, Yingguo Bai, Novel Fungal Immunomodulatory Protein FIP-NHA With Antineoplastic Activity And Gene Thereof, Institute of Animal Science of CAAS, China, 2011.
- [24] S. Bastiaan-Net, W. Chanput, A. Hertz, R.D. Zwiittink, J.J. Mes, H.J. Wichers, Biochemical and functional characterization of recombinant fungal immunomodulatory proteins (rFIPs), *Int. Immunopharmacol.* 15 (1) (2013) 167–175.
- [25] Y. Xie, S. Li, L. Sun, S. Liu, F. Wang, B. Wen, L. Sun, X. Fang, Y. Cha, H. Cao, N. Jia, T. Gu, X. Lou, F. Xin, Fungal immunomodulatory protein from *Nectria haematococca* suppresses growth of human lung adenocarcinoma by inhibiting the PI3K/Akt pathway, *Int. J. Mol. Sci.* 19 (11) (2018).
- [26] S. Li, Y. Nie, Y. Ding, L. Shi, X. Tang, Recombinant expression of a novel fungal immunomodulatory protein with human tumor cell antiproliferative activity from *Nectria haematococca*, *Int. J. Mol. Sci.* 15 (10) (2014) 17751–17764.
- [27] B. Yao H. Zhao S. Li H. Luo K. Meng P. Yang Y. Wang H. Huang P. Shi T. Yuan Y. Bai Novel fungal immunomodulatory protein FIP-NHA with antineoplastic activity and gene thereof CN102241751A 2011.
- [28] S.-Y. Li, L.-Z. Hou, Y.-X. Gao, N.-N. Zhang, B. Fan, F. Wang, FIP-nha, a fungal immunomodulatory protein from *nectria haematococca*, induces apoptosis and autophagy in human gastric cancer cells via blocking the EGFR-mediated STAT3/Akt signaling pathway, *Food Chem.Mol.Sci.* 4 (2022).
- [29] J.-J. Wang, Y. Wang, L. Hou, F. Xin, B. Fan, C. Lu, L. Zhang, F. Wang, S. Li, Immunomodulatory protein from induces apoptosis in lung cancer cells via the P53 pathway, *Int. J. Mol. Sci.* 20 (21) (2019).
- [30] H. Han, Z. Ling, A. Khan, A.K. Virk, S. Kulshrestha, X. Li, Improvements of thermophilic enzymes: from genetic modifications to applications, *Bioresour. Technol.* 279 (2019) 350–361.
- [31] W.F. Li, X.X. Zhou, P. Lu, Structural features of thermozyms, *Biotechnol. Adv.* 23 (4) (2005) 271–281.
- [32] Z. Xu, Y.-K. Cen, S.-P. Zou, Y.-P. Xue, Y.-G. Zheng, Recent advances in the improvement of enzyme thermostability by structure modification, *Crit. Rev. Biotechnol.* 40 (1) (2020) 83–98.
- [33] R. Han, G. Xu, J. Dong, Y. Ni, Arginine deiminase: recent advances in discovery, crystal structure, and protein engineering for improved properties as an anti-tumor drug, *Appl. Microbiol. Biotechnol.* 100 (11) (2016) 4747–4760.
- [34] L. Zhu, F. Cheng, V. Piatkowski, U. Schwaneberg, Protein engineering of the antitumor enzyme PpADI for improved thermal resistance, *ChemBioChem* 15 (2) (2014) 276–283.
- [35] M. Li, R. Zhao, J. Chen, W. Tian, C. Xia, X. Liu, Y. Li, S. Li, H. Sun, T. Shen, W. Ren, L. Sun, Next generation of anti-PD-L1 Atelizumab with enhanced anti-tumor efficacy in vivo, *Sci. Rep.* 11 (1) (2021) 5774.
- [36] C.-H. Tung, C.-C. Lin, H.-J. Wang, S.-F. Chen, F. Sheu, T.-J. Lu, Application of thermal stability difference to remove flammutoxin in fungal immunomodulatory protein, FIP-fve, extract from *Flammulina velutipes*, *J. Food Drug Anal.* 26 (3) (2018) 1005–1014.
- [37] W. Huang, C. Yang, D. Chen, L. Chuang, Correlation of the structure and bioactivity of recombinant fungal immunomodulatory protein, Ling-Zhi-8 (LZ-8) following exposure to denaturing conditions, *J. Food Biochem.* 38 (3) (2014) 328–336.
- [38] M. An, G.F. Gao, J. Qi, F. Li, X. Liu, Expression and crystallographic studies of a fungal immunomodulatory protein LZ-8 from a medicinal fungus *Ganoderma lucidum*, *Sheng Wu Gong Cheng Xue Bao* 26 (11) (2010) 1563–1568.
- [39] M.-Y. Wu, M.-F. Hsu, C.-S. Huang, H.-Y. Fu, C.-T. Huang, C.-S. Yang, A 2.0 Å structure of GMI, a member of the fungal immunomodulatory protein family from *Ganoderma microsporum*, *Protein Crystallogr.* II-132 (2007).
- [40] S.V. Seow, I.-C. Kuo, P. Paaventhan, P.R. Kolatkar, K.Y. Chua, Crystallization and preliminary X-ray crystallographic studies on the fungal immunomodulatory protein fve from the golden needle mushroom (*Flammulina velutipes*), *Acta Crystallogr. D* 59 (Pt 8) (2003) 1487–1489.
- [41] P. Paaventhan, J.S. Joseph, S.V. Seow, S. Vaday, H. Robinson, K.Y. Chua, P. R. Kolatkar, A 1.7Å structure of Fve, a member of the new fungal immunomodulatory protein family, *J. Mol. Biol.* 332 (2) (2003) 461–470.
- [42] X. Liu, T. Liu, Y. Zhang, F. Xin, S. Mi, B. Wen, T. Gu, X. Shi, F. Wang, L. Sun, Structural insights into the thermophilic adaption mechanism of endo-1,4-β-xylanase from *Caldicellulosiruptor owensensis*, *J.Agric.Food Chem.* 66 (1) (2018) 187–193.
- [43] S. Harper, D.W. Speicher, Expression and purification of GST fusion proteins, Chapter 6, *Curr. Protoc. Protein Sci.* (2008), <https://doi.org/10.1002/0471140864.ps0606s09>. Unit 6.6.
- [44] D. Berek, Size exclusion chromatography—a blessing and a curse of science and technology of synthetic polymers, *J. Sep. Sci.* 33 (3) (2010) 315–335.
- [45] J.L. Brunelle, R. Green, One-dimensional SDS-polyacrylamide gel electrophoresis (1D SDS-PAGE), *Methods Enzymol.* 541 (2014) 151–159.
- [46] M.R. Jacobs, M. Grace, A. Blumlein, J.J. McManus, Differential scanning calorimetry to quantify heat-induced aggregation in concentrated protein solutions, *Methods Mol. Biol.* 2039 (2019) 117–129.
- [47] Y. Chang, Y. Hsiao, M. Wu, C. Ou, Y. Lin, K. Lue, J. Ko, Interruption of lung cancer cell migration and proliferation by fungal immunomodulatory protein FIP-fve from *Flammulina velutipes*, *J.Agric.Food Chem.* 61 (49) (2013) 12044–12052.
- [48] Z. Otwinowski, W. Minor, Processing of X-ray diffraction data collected in oscillation mode, *Meth. Enzymol.* 276 (1997) 307–326.
- [49] M.A. Hough, K.S. Wilson, From crystal to structure with CCP4, *Acta Crystallogr. Sect. D Struct. Biol.* 74 (Pt 2) (2018) 67.
- [50] P.D. Adams, R.W. Grosse-Kunstleve, L.W. Hung, T.R. Ioerger, A.J. McCoy, N. W. Moriarty, R.J. Read, J.C. Sacchettini, N.K. Sauter, T.C. Terwilliger, PHENIX: building new software for automated crystallographic structure determination, *Acta Crystallogr. D* 58 (Pt 11) (2002) 1948–1954.
- [51] P. Emsley, K. Cowtan, Coot: model-building tools for molecular graphics, *Acta Crystallogr. D* 60 (Pt 12 Pt 1) (2004) 2126–2132.
- [52] U.C. Ejike, C.J. Chan, P.N. Okechukwu, R.L.H. Lim, New advances and potentials of fungal immunomodulatory proteins for therapeutic purposes, *Crit. Rev. Biotechnol.* 40 (8) (2020) 1172–1190.
- [53] S.D. Story, S. Boggs, L.M. Guiney, M. Ramesh, M.C. Hersam, C.J. Brinker, S. L. Walker, Aggregation morphology of planar engineered nanomaterials, *J. Colloid Interface Sci.* 561 (2020) 849–853.
- [54] A.P. Minton, Static light scattering from concentrated protein solutions, I: general theory for protein mixtures and application to self-associating proteins, *Biophys. J.* 93 (4) (2007) 1321–1328.
- [55] C.-H. Lin, Y.-M. Hsiao, C.-C. Ou, Y.-W. Lin, Y.-L. Chiu, K.-H. Lue, J.-G. Chang, J.-L. Ko, GMI, a *Ganoderma* immunomodulatory protein, down-regulates tumor necrosis factor alpha-induced expression of matrix metalloproteinase 9 via NF-kappaB pathway in human alveolar epithelial A549 cells, *J.Agric.Food Chem.* 58 (22) (2010) 12014–12021.
- [56] S. Ghasemi, S. Davaran, S. Sharifi, D. Asgari, A. Abdollahi, J. Shahbazi Mojarad, Comparison of cytotoxic activity of L778123 as a farnesyltransferase inhibitor and doxorubicin against A549 and HT-29 cell lines, *Chem. Pharm. Bull.* 3 (1) (2013) 73–77.
- [57] L.J. Lalitha, T.J. Sales, P. Prince, P. Clarence, Y.-O. Agastian, A.H. Kim, M. S. Mahmoud, J.C. Elshikh, S.W. Tack, H.-J. Kim Na, In-vitro phytopharmacological and anticancer activity of *Loranthus Longiflorus* Desv. Var. *Falcatu* against the human lung cancer cells, *J. King Saud Univ. Sci.* 32 (2020) 1246–1253.
- [58] C. Carvalho, R.X. Santos, S. Cardoso, S. Correia, P.J. Oliveira, M.S. Santos, P. I. Moreira, Doxorubicin: the good, the bad and the ugly effect, *Curr. Med. Chem.* 16 (25) (2009) 3267–3285.
- [59] H. Berman, K. Henrick, H. Nakamura, Announcing the worldwide protein data Bank, *Nat. Struct. Biol.* 10 (12) (2003) 980.
- [60] Y.F. Liu, S.H. Chang, H.L. Sun, Y.C. Chang, L.L. Hsin, K.H. Lue, J.L. Ko, IFN-gamma induction on carbohydrate binding module of fungal immunomodulatory protein in human peripheral mononuclear cells, *J. Agric. Food Chem.* 60 (19) (2012) 4914–4922.
- [61] H. Nishimasu, S. Fushinobu, H. Shoun, T. Wakagi, The first crystal structure of the novel class of fructose-1,6-bisphosphatase present in Thermophilic archaea, *Structure* 12 (6) (2004) 949–959.
- [62] J. Huang, H. Fang, Z. Gai, J. Mei, J. Li, S. Hu, C. Lv, W. Zhao, L. Mei, *Lactobacillus brevis* CGMCC 1306 glutamate decarboxylase: crystal structure and functional analysis, *Biochem.Biophys.Res.Comm.* 503 (3) (2018) 1703–1709.
- [63] G. Luo, X. Zhu, Y. Lv, B. Lv, J.E. Fang, S. Cao, H. Chen, G. Peng, Y. Songa, Crystal structure of the dimerized N terminus of porcine coronavirus type 2 replicase protein reveals a novel antiviral interface, *J. Virol.* 92 (18) (2018).
- [64] E. Krissinel, K. Henrick, Inference of macromolecular assemblies from crystalline state, *J. Mol. Biol.* 372 (3) (2007) 774–797.
- [65] W.-H. Lin, C.-H. Hung, C.-I. Hsu, J.-Y. Lin, Dimerization of the N-terminal amphipathic alpha-helix domain of the fungal immunomodulatory protein from *Ganoderma tsugae* (Fip-gts) defined by a yeast two-hybrid system and site-directed mutagenesis, *J. Biol. Chem.* 272 (32) (1997) 20044–20048.
- [66] C.-C. Ou, Y.-M. Hsiao, W.-H. Wang, J.-L. Ko, M.-Y. Lin, Stability of fungal immunomodulatory protein, FIP-gts and FIP-fve, in IFN-γ production, *Food Agric. Immunol.* 20 (4) (2009) 319–332.
- [67] D.-P. Bao, R. Bai, Y.-N. Gao, Y.-Y. Wu, Y. Wang, Computational insights into the molecular mechanism of the high immunomodulatory activity of LZ-8 protein isolated from the Lingzhi or Reishi medicinal mushroom *ganoderma lucidum* (Agaricomycetes), *Int. J. Med. Mushrooms* 20 (6) (2018) 537–548.
- [68] V. Pushparajah, A. Fatima, C.H. Chong, T.Z. Gambule, C.J. Chan, S.T. Ng, C.S. Tan, S.Y. Fung, S.S. Lee, N.H. Tan, R.L.H. Lim, Characterisation of a new fungal immunomodulatory protein from tiger milk mushroom, *Lignosus rhinocerotis*, *Sci. Rep.* 6 (2016) 30010.
- [69] C.-H. Liao, Y.-M. Hsiao, C.-P. Hsu, M.-Y. Lin, J.C.-H. Wang, Y.-L. Huang, J.-L. Ko, Transcriptionally mediated inhibition of telomerase of fungal immunomodulatory protein from *Ganoderma tsugae* in A549 human lung adenocarcinoma cell line, *Mol. Carcinog.* 45 (4) (2006) 220–229.
- [70] C.-H. Liao, Y.-M. Hsiao, G.-T. Sheu, J.T. Chang, P.-H. Wang, M.-F. Wu, G.-J. Shieh, C.-P. Hsu, J.-L. Ko, Nuclear translocation of telomerase reverse transcriptase and calcium signaling in repression of telomerase activity in human lung cancer cells by fungal immunomodulatory protein from *Ganoderma tsugae*, *Biochem. Pharmacol.* 74 (10) (2007) 1541–1554.
- [71] S. Li, Z. Jiang, W. Xu, Y. Xie, L. Zhao, X. Tang, F. Wang, F. Xin, FIP-sch2, a new fungal immunomodulatory protein from *stachybotrys chlorohalonata*, suppresses proliferation and migration in lung cancer cells, *Appl.Microbiol.Biotechnol.* 101 (8) (2017) 3227–3235.
- [72] S. Li, Z. Jiang, L. Sun, X. Liu, Y. Huang, F. Wang, F. Xin, Characterization of a new fungal immunomodulatory protein, FIP-dsq2 from *Dichomitus squalens*, *J. Biotechnol.* 246 (2017) 45–51.
- [73] S. Zhou, S. Guan, Z. Duan, X. Han, X. Zhang, W. Fan, H. Li, L. Chen, H. Ma, H. Liu, Y. Ruan, J. Lin, Molecular cloning, codon-optimized gene expression, and bioactivity assessment of two novel fungal immunomodulatory proteins from

- Ganoderma applanatum in Pichia, Appl. Microbiol. Biotechnol. 102 (13) (2018) 5483–5494.
- [74] Y. Wang, Y. Gao, R. Bai, H. Chen, Y. Wu, J. Shang, D. Bao, Identification of a novel anti-cancer protein, FIP-bbo, from Botryobasidium botryosum and protein structure analysis using molecular dynamic simulation, Sci. Rep. 9 (1) (2019) 5818.
- [75] Z. Qu, S. Zhou, S. Guan, R. Gao, Z. Duan, X. Zhang, W. Sun, W. Fan, S. Chen, L. Chen, J. Lin, Y. Ruan, Recombinant expression and bioactivity comparison of four typical fungal immunomodulatory proteins from three main Ganoderma species, BMC Biotechnol. 18 (1) (2018) 80.